AGU PUBLICATIONS

JGR

Journal of Geophysical Research: Oceans

RESEARCH ARTICLE

10.1002/2014JC010239

Spatial variances of wind fields and their relation to second-order structure functions and spectra

Jur Vogelzang[1], Gregory P. King[2,3,4,5], and Ad Stoffelen[1]

[1]KNMI Royal Netherlands Meteorological Institute, De Bilt, Netherlands, [2]Centro de Geofisica—IDL, Universidade de Lisboa, Lisboa, Portugal, [3]Now at Institut de Ciències del Mar — CSIC, [4]Institut de Ciències del Mar—CSIC, Barcelona, Spain, [5]School of Marine Sciences, Nanjing University of Information Science and Technology, Nanjing, China

Key Points:
- Spatial variances V provide good estimate of variance versus scale
- Wind spectra and structure functions D give rough estimate of variance vs scale
- When D obeys a power law with exponent p the ratio D/V equals $(p+1)$ $(p+2)$

Correspondence to:
J. Vogelzang,
jur.vogelzang@knmi.nl

Citation:
Vogelzang, J., G. P. King, and A. Stoffelen (2015), Spatial variances of wind fields and their relation to second-order structure functions and spectra, *J. Geophys. Res. Oceans*, *120*, 1048–1064, doi:10.1002/2014JC010239.

Received 13 JUN 2014
Accepted 23 JAN 2015
Accepted article online 29 JAN 2015
Published online 20 FEB 2015

Abstract Kinetic energy variance as a function of spatial scale for wind fields is commonly estimated either using second-order structure functions (in the spatial domain) or by spectral analysis (in the frequency domain). Both techniques give an order-of-magnitude estimate. More accurate estimates are given by a statistic called spatial variance. Spatial variances have a clear interpretation and are tolerant for missing data. They can be related to second-order structure functions, both for discrete and continuous data. Spatial variances can also be Fourier transformed to yield a relation with spectra. The flexibility of spatial variances is used to study various sampling strategies, and to compare them with second-order structure functions and spectral variances. It is shown that the spectral sampling strategy is not seriously biased to calm conditions for scatterometer ocean surface vector winds. When the second-order structure function behaves like r^p, its ratio with the spatial variance equals $(p+1)(p+2)$. Ocean surface winds in the tropics have p between 2/3 and 1, so one-sixth to one-fifth of the second-order structure function value is a good proxy for the cumulative variance.

1. Introduction

The variance contained in wind fields at different scales plays a central role in various branches of geophysics and meteorology, as it is directly related to the turbulent kinetic energy [e.g., *Frisch*, 1995 or any other text book on turbulence]. Moreover, small-scale turbulence is parameterized in Numerical Weather Prediction (NWP) models and determines the amount of subgrid mixing and constituent transport. In addition, scale-dependent variance determines the representation error contribution to observation errors in NWP data assimilation [e.g., *Lorenc*, 1986; *Frehlich*, 2001] and dominates the *in situ* observation wind error (e.g., from buoys, radiosondes). Spectral analysis has been applied to quantify the amount of small-scale structure in the wind field using winds measured from aircraft [e.g., *Nastrom and Gage*, 1985] and derived from satellite observations [e.g., *Freilich and Chelton*, 1986; *Patoux and Brown*, 2001]. Differences in variance content between scatterometer observations and NWP model predictions have been used to estimate the representation error in triple collocation studies [*Vogelzang et al*., 2011]. Moreover, spectral techniques are used to simulate turbulent fields spatially [*Frehlich et al*., 2001].

Spectral analysis is the standard method for calculating variance as a function of scale. The spectrum gives the variance density as a function of wave number k and the variance contained in the wave number interval (k_1, k_2) equals the integral over the spectrum between these limits. The spatial scale associated with k is $r=1/k$ (assuming a Fourier transformation factor $e^{2\pi ikr}$), so often the cumulative variance at scale r is taken as the integral of the spectrum from $k=1/r$ to infinity. However, this interpretation is not correct, because the Fourier modes have no sharp spatial representation. Further, spectral analysis based on Fast Fourier Transform (FFT) techniques requires samples without missing points, which is a serious drawback in many practical applications. In the case of scatterometer ocean surface winds, *Vogelzang et al*. [2011] find that for winds on a 25 km grid with a sample size of 128 points (sample length 3200 km) only about 6% of the data falls into samples without missing points. If isolated missing points are replaced by interpolated winds, about 35% of the data is used, thus discarding two-thirds of the data. Missing scatterometer winds are often associated with highly dynamic features such as fronts and cyclone centers [*Stoffelen and Anderson*, 1997]. In consequence, the results of spectral analysis may be biased to calm conditions. Another complication is that Fast Fourier Transform (FFT) algorithms assume the sample to be periodic. For wind spectra in the

Earth's atmosphere one must apply a detrending method to minimize the difference between the first and last point of the sample, otherwise a k^{-2} contribution to the spectrum would be introduced that dominates at high wave numbers (small scales). Detrending has no effect on the spectrum at medium to large wave numbers [*Vogelzang et al*., 2011], and its effect on nonzero wave numbers can be completely corrected for by using first differences [*Percival and Walden*, 1993]. Finally, the spectral density is given on an equidistant wave number grid. When transformed to position space, the spatial grid points concentrate at the smallest scales.

Second-order structure functions (second moments of velocity differences) are defined in position space and their calculation easily accommodates missing data. Often the variance contained within a certain scale is set equal to half the structure function value at that scale. However, as emphasized by *Davidson and Pearson* [2005], this relation is only approximate. A more precise relation will be presented in this paper and it will be shown that one-fifth to one-sixth of the structure function value is a good proxy for the variance, at least for ocean surface winds in the Tropical Pacific.

Wind spectra and second-order structure functions only give an order-of-magnitude estimation of variance as a function of scale. In an attempt to find a more accurate estimate, a statistic called spatial variance is reintroduced. It is the sample variance averaged over all samples as a function of sample length [*Yates*, 1948]. Spatial variances have a clear interpretation and are tolerant for missing data. Nevertheless, their use is not widespread. In metrology literature (not to be confused with meteorology), it is known as M-sample variance [*Allan*, 1966]. For two-point samples it is called Allan variance, for three-point samples Hadamard variance. Spatial variance (also referred to as blocked quadrat variance) has been used by *Kahn and Teixeira* [2009] to estimate spatial length scale exponents for temperature and water vapor derived from infrared satellite observations. *Mahadevan and Campbell* [2002] use spatial variance in two dimensions to characterize spatial heterogeneity of tracers in oceanography, restricting their analysis to domains of size L, $L/2$, $L/4$, etc. A two-dimensional version of spatial variance is used by *Blue and Chen* [2011] for controlling and optimizing wafer spatial variations in integrated circuit fabrication.

Lorenz [1979] introduced the "poor man's spectral analysis," a method to construct the spectrum from spatial variances at scales that are a fraction 2^{-n} of the sample size, with n an integer, taking into account the Fourier transform properties when transforming from the frequency domain to the spatial domain [see also *Cahalan et al*., 1994] for a more complete description). This bears some resemblance to spatial variance, but, as indicated by the name, the emphasis of "poor man's spectral analysis" is in the frequency domain, whereas that of spatial variance is in the spatial domain.

For data sets without missing points spatial variance is related to the second-order structure function. For a single series of discrete data, this relationship appears to have been first recognized by *Yates* [1948]. It is easily generalized to the continuous case by letting the sampling distance approach zero. Moreover, since the relation holds for any data series that is long enough, it also must hold for ensemble averages – provided that velocity differences converge to structure functions under ensemble averaging (see Appendix A for details). The complement of spatial variance can be Fourier transformed and related to the wind spectrum, as shown in Appendix B.

For data sets with missing points the sampling strategy becomes important. Spatial variances are flexible enough to cope with a number of sampling strategies, thus enabling to study their effect, in particular for those strategies that are commonly used in spectral or spatial analysis.

The aim of the paper is threefold: (i) to (re)introduce spatial variance as a more precise estimate of variance as a function of scale, (ii) to study the effect of sampling strategy on spatial variance, and (iii) to compare spatial variances with spectral variances and second-order structure functions. The paper is organized as follows: in section 2 the relevant definitions of spectra and structure functions are presented. The problems with their relation to variance as a function of spatial scale are discussed. It will be shown why qualitative arguments based on the interpretation of the spectrum as a variance density are correct. In section 3, spatial variances are defined and related to second-order structure functions and spectra. Several sampling strategies are presented in section 4. In section 5, some results are presented for scatterometer ocean surface vector winds. The effect of sampling strategy on spatial variance is investigated. Spatial variances are compared with spectral variances and second-order structure functions. It is shown that one-fifth to one-sixth of the second-order structure function value is a good proxy for the cumulative kinetic energy, in accordance with simple power-

law behavior of second-order structure functions, r^p, and spectra, k^{-p-1}, with p between 2/3 and 1 or slightly more. It is also shown that spectral sampling is not seriously biased to calm wind conditions. The paper ends with the conclusions in section 6. Appendix A contains the derivation of the relation between spatial variance and second-order structure functions, Appendix B that between spatial variance and spectrum.

2. Spectra and Second-Order Structure Functions

Past studies have shown that in the upper troposphere and lower stratosphere wind spectra show the classical Kolmogorov $k^{-5/3}$ behavior for wave numbers above 10^{-6} m^{-1} [*Nastrom and Gage*, 1985], while for lower wavenumbers a k^{-3} behavior is found. Spectra of ocean surface wind components calculated from scatterometer measurements are slightly steeper [*Freilich and Chelton*, 1986; *Patoux and Brown*, 2001; *Vogelzang et al.*, 2011], with exponents up to -2.4. Ocean surface wind spectra show no sign of transition to exponent -3 for low wavenumbers.

In practical applications, spectra and structure functions are generally defined for equally spaced finite data sets. Suppose we have a data set $\{u_i\}=\{u(x_i)\}$ with $x_i=i\Delta x$, $i=0,1,\cdots,N$. Suppose also, for the moment, that the data set does not contain missing points.

2.1. Spectra

Divide the data set into a number of nonoverlapping subsets, further referred to as samples, each containing n points indexed within the sample from 0 to $n-1$. For each sample a periodogram $\psi_s(k_j)$, with s the sample index, can be defined in two equivalent ways [*Press et al.*, 1988]: as the absolute value squared of the discrete Fourier transform of the values in the sample,

$$\psi_s(k_j)=\left|\sum_{l=0}^{n-1} u_l e^{2\pi i \frac{jl}{n}}\right|^2, \tag{1}$$

or as the discrete Fourier transform of the autocovariance function A_s of the sample,

$$\psi_s(k_j)=\sum_{l=0}^{n-1} A_s(l) e^{2\pi i \frac{jl}{n}}, \tag{2}$$

where

$$A_s(l)=\frac{1}{n}\sum_{j=0}^{n-1} u_j u_{j+l}, \tag{3}$$

and the indices are to be taken modulo n. The periodogram is given at discrete frequencies

$$k_j=\frac{j}{n\Delta x}, \quad j=-\frac{n}{2},\cdots,\frac{n}{2}. \tag{4}$$

The periodogram $\psi_s(k_j)$ is normalized such that its sum over all nonzero frequencies k_j equals the variance of the sample, $\sigma_s^2(n)$,

$$\sigma_s^2(n)=\sum_{\substack{j=-n/2\\ j\neq 0}}^{n/2} \psi_s(k_j). \tag{5}$$

In deriving (5) one must use the fact that a discrete Fourier transformation assumes the samples to be cyclic, and that the periodogram at zero frequency equals the square of the sample average of u.

As the periodogram is a very noisy estimator, the spectrum is in most cases the average of a sufficient number of periodograms. For real signals the autocovariance is real and even, and so is its periodogram. One may therefore project the negative frequencies on the positive ones, resulting in a spectrum $\Psi(k_j)$ that is a function of nonnegative frequencies only. Since the spectrum is the average of all periodograms, summing the spectrum over all frequencies yields the mean of the sample variances, $\sigma^2(n)$, as

$$\sigma^2(n)=\frac{1}{S}\sum_{s=1}^{S}\sigma_s^2(n), \tag{6}$$

where S is the number of samples. Note that $\sigma^2(n)$ is not the variance of the whole data set but the average value of the variance for scale $n\Delta x$ as indicated by the argument n.

Associating a spatial scale r_m with the wavenumber k_m by $r_m=1/k_m$, the variance contained in scales up to r_m, denoted as $\sigma^2(m,n)$, is often written as

$$\sigma^2(m,n)=\sum_{j=m}^{n/2}\Psi(k_j)=\sum_{j=-n/2}^{n/2}\psi(k_j)\hat{w}(j;m), \tag{7}$$

where we introduced a high pass filter $\hat{w}(j;m)$ that equals 1 for $|j|\geq m$ and zero elsewhere in order to extend the summation to all frequencies. Moreover, we assume for convenience that the average has been removed from each sample to have $\psi(0)=0$; as a result the summation index can take also the value 0. Finally, we made use of the fact that all indices should be taken modulo n. After application of (2) and the introduction of the inverse Fourier transform of $\hat{w}$ in the right-hand side of (7), we can change the order of summations and perform the summation over j which yields a Kronecker delta. The result is

$$\sigma^2(m,n)=\sum_{l=0}^{n-1}A(l)w(l;m), \tag{8}$$

with A the autocovariance averaged over all samples and with the inverse Fourier transform w of the high-pass filter given by the discrete analogue of a sinc function

$$w(l;m)=\sum_{j=-m/2}^{m/2}e^{2\pi i\frac{jl}{n}}. \tag{9}$$

Equation (8) shows that the discrete spectrum summed over a partial interval does not transform to a variance in the spatial domain, but to a sum of autocovariances weighted with an oscillating function. The same argument holds for continuous infinite spectra.

The conclusion is that one should be careful when translating spectral results to the spatial domain. In particular, the variance $\sigma^2(m,n)$ in (7) cannot be attributed to a sharply defined spatial scale r_m.

Nevertheless, autocovariance and variance are related: if a data set contains much small scale detail, its autocovariance will be a narrow function. The spectrum, being the Fourier transform of the autocovariance, will be a broad function, and the spectral density at small scales (large frequencies) will be high. Therefore, qualitative arguments based on the interpretation of the spectrum as a variance density are correct.

2.2. Structure Functions

Structure functions are defined as averages over velocity increments $\delta u_n=u_i-u_{i+n}$, where u is the wind component parallel or perpendicular to the line connecting points x_i and x_{i+n}, denoted as l and t, respectively. Here, each pair (u_i,u_{i+n}) can be considered as the end points of a sample with $n+1$ points and lag size n (distance between first and last point in units of the grid size Δx). Note that we changed the notation of the sample size compared to that in the previous paragraph, because it is more convenient to work now in terms of lags. The second-order structure functions satisfy

$$D_{ll}(n)=\langle(\delta l_n)^2\rangle,\quad D_{tt}(n)=\langle(\delta t_n)^2\rangle, \tag{10}$$

where the brackets $\langle.\rangle$ denote ensemble averaging. Ensemble averaging converges for ocean surface wind components, because the spectra follow a power law with exponent between -3 and -1. In geophysical applications like the one considered in this study one must rely on ergodicity which states that ensemble averages may be replaced by series averages,

$$D_{ll}(n)=E\left[(\delta l_n)^2\right],\quad D_{tt}(n)=E\left[(\delta l_{tt})^2\right], \tag{11}$$

where E is the expectation operator that denotes averaging over all samples in a single data series. From the definition of the velocity increments and (11) it is easily shown that

$$D_{ll}(n)=2\sigma_l^2(n)[1-\rho_{ll}(n)], \quad D_{tt}(n)=2\sigma_t^2(n)[1-\rho_{tt}(n)], \tag{12}$$

where $\sigma_l^2(n)=E\left[l_i^2\right]=E\left[l_{i+n}^2\right]$, $\sigma_t^2(n)=E\left[t_i^2\right]=E\left[t_{i+n}^2\right]$. The autocorrelations ρ_{ll} and ρ_{tt} are normalized autocovariances defined as

$$\rho_{ll}(n)=\frac{A_{ll}(n)}{\sigma_l^2(n)}, \quad \rho_{tt}(n)=\frac{A_{tt}(n)}{\sigma_t^2(n)}. \tag{13}$$

with A_{ll} and A_{tt} defined in (3), and $\rho_{ll}(0)=\rho_{tt}(0)=1$. For large values of n, i.e., large distances, one expects the autocorrelation to go to zero and (12) yields

$$\sigma_l^2(n)=\frac{1}{2}D_{ll}(n), \quad \sigma_t^2(n)=\frac{1}{2}D_{tt}(n). \tag{14}$$

This explains why the second-order structure function is called the semivariogram in geostatistics. Wind fields are correlated up to planetary scale, so (14) can only be approximate. Moreover, if one takes $n=1$ (neighboring points), the variance of a sample is defined as

$$\sigma_l^2(1)=\frac{1}{2}\left[(l_i-\bar{l})^2+(l_{i+1}-\bar{l})^2\right], \tag{15}$$

with $\bar{l}=\frac{1}{2}(l_i+l_{i+1})$ the average velocity. Expanding yields

$$\sigma_l^2(1)=\frac{1}{4}(l_i-l_{i+1})^2, \tag{16}$$

and a similar equation holds for $\sigma_t^2(1)$. Averaging over all samples yields for neighboring points

$$\sigma_l^2(1)=\frac{1}{4}D_{ll}(1), \quad \sigma_t^2(1)=\frac{1}{4}D_{tt}(1). \tag{17}$$

This differs by a factor of 2 from (14), another indication that the second-order structure function gives an order-of-magnitude estimate of variance as a function of scale.

3. Spatial Variances

3.1. Definition

To get a more reliable measure of the variance as a function of scale we introduce quantities we call spatial variances. As noted before, spatial variances are sample variances averaged over all samples as a function of sample length. From the point of numerical calculation, the most convenient way to define them is through first and second moments. For wind components l and t the spatial variances V_l and V_t read

$$V_l(n)=E\left[M_{ll}(n)-M_l^2(n)\right], \quad V_t(n)=E\left[M_{tt}(n)-M_t^2(n)\right], \tag{18}$$

with the expectation operator E defined as before and the first and second moments defined as

$$M_l(n)=\frac{1}{n+1}\sum_{j=0}^{n}l_{i+j}, \quad M_{ll}(n)=\frac{1}{n+1}\sum_{j=0}^{n}l_{i+j}^2, \tag{19}$$

with similar definitions for t. Equations (18) and (19) are a generalization of (15). The data set is divided into samples each containing $n+1$ points, the variance over each sample is calculated, and all variances are averaged. This is repeated for all values of n that are of interest. The samples may be overlapping or not (see section 4). The spatial variance defined in (18) and (19) is tolerant of missing points, i.e., it is not necessary to reject a sample when it contains missing points; this in contrast with spectral calculations. In (19) one can simply neglect these points, the minimum requirement being that the sample contains at least 2 valid (non-missing) points. Therefore, all measurement points may in principle be considered when computing spatial variances according to (18) and (19). How one exactly deals with the missing points is part of the sampling strategy adopted, and that influences the results. Note that the spatial variance involves all valid points in a sample, not only the end points. Spatial variances are not spuriously sensitive to large-scale fluctuations (low wave number spectral components) because the variance of each sample is taken with respect to the

sample mean. The spatial variance of a well-behaving signal will go to infinity with the number of sample points, reflecting the fact that a signal with finite power but infinite duration contains infinite energy.

3.2. Relation With Second-Order Structure Functions

As shown in Appendix A, the spatial variance can be related to the second-order structure function, and vice versa, by [*Yates*, 1948]

$$V(n)=\frac{1}{(n+1)^2}\sum_{m=1}^{n}(n+1-m)D(m), \tag{20}$$

$$D(n)=(n+1)^2V(n)-2n^2V(n-1)+(n-1)^2V(n-2), \tag{21}$$

where the subscript indicating the wind component under consideration has been suppressed.

These relations are statistically exact for a single data series that is free of missing points and large enough to ensure convergence to a uniform $D(m)$. Since no restriction is imposed on the data series (except the trivial one that all data values are finite), it must also hold for ensemble averages in cases where velocity differences converge to structure functions; see Appendix A for details.

When $V(n)$ is a rising function of n the relation $V(n-2) \le V(n-1) \le V(n)$ holds, and substitution in (21) immediately gives $D(n) \le 2V(n)$, implying that in such cases $D(n)$ is always smaller than two times the spatial variance. Relations (20) and (21) confirm that the spatial variances are insensitive to large-scale fluctuations, just like the second-order structure functions.

In the continuous case (20) and (21) become

$$V(r)=\frac{1}{r^2}\int_0^r ds(r-s)D(s), \tag{22}$$

$$D(r)=r^2\frac{d^2V(r)}{dr^2}+4r\frac{dV(r)}{dr}+2V(r). \tag{23}$$

Note that the continuous equivalent of equation (14) results from (23) if the first and second derivatives of the spatial variance vanish for large r, i.e., when the spatial variance becomes constant for large r, or, equivalently, when the autocorrelation vanishes.

The spatial variance $V(r)$, measures the cumulative turbulent kinetic energy over a scale r, as is obvious from its definition. The energy contained in a range of scales (r_1, r_2) is therefore $V(r_2)-V(r_1)$. This can be written as an integral from r_1 to r_2 of the derivative of $V(r)$ that can be found from (22) as

$$\frac{dV(r)}{dr}=\frac{1}{r^2}\int_0^r ds(2s-r)D(s). \tag{24}$$

The derivative of $V(r)$ can thus be interpreted as a variance density in position space.

Note that when the second-order structure function is given by a simple power law $D(r)=Cr^p$, with C a constant and $p > -1$, substitution into (22) and integration yields

$$V(r)=\frac{Cr^p}{(p+1)(p+2)}. \tag{25}$$

This leads to

$$\frac{D(r)}{V(r)}=(p+1)(p+2). \tag{26}$$

3.3. Relation With the Spectrum

It is not possible to directly Fourier transform the spatial variance, because $V(r)$ approaches σ^2, the total variance, as r goes to infinity. Therefore the Fourier integral for the zero frequency component does not exist. The same argument applies to second-order structure functions, but there their complement (up to a factor

2), the autocovariance, possesses a Fourier transform, see (12) and (13). Analogously, define the complement of the spatial variance, denoted as $\bar{V}(r)$, by $V(r)+\bar{V}(r)=\sigma^2$, assuming that σ^2 is finite. One can recognize $\bar{V}(r)$ immediately as the variance contained in all scales larger than r. In Appendix B it is shown that

$$\psi(k)=\frac{1}{2}\frac{k^2d^2\hat{\bar{V}}(k)}{dk^2}\frac{-2kd\hat{\bar{V}}(k)}{dk}+\hat{\bar{V}}(k), \tag{27}$$

with $\hat{\bar{V}}(k)$ the Fourier transform of $\bar{V}(r)$. Equation (27) will not be investigated further in this paper, but is included for the sake of completeness. Moreover, it assumes finite total variance.

Note that numerical calculation of $\hat{\bar{V}}(k)$ is plagued by the same practical problems as that of $\psi(k)$, see section 2.1. In particular, some form of detrending will be needed, whereas the nice feature of spatial variance is that it can do without detrending.

4. Sampling Strategy

The spatial variance as defined in (18) depends on the sampling strategy adopted, and when comparing it with spectral estimates based on (5) or with structure function estimates based on (20) the sampling should be properly taken into account.

In the first place one may choose between overlapping or consecutive (nonoverlapping) samples. The first choice is commonly made for calculating structure functions, while the second one is customary for calculating spectra.

Second, one may choose if missing points are allowed in a sample, and if so, how many. The number of missing points allowed can be characterized by the maximum fraction of missing points, $f_{\max}$. A sample of length $n+1$ is rejected when the number of missing points m is such that $m/(n+1) > f_{\max}$. With $f_{\max}=1$ all points are accepted (with the absolute minimum requirement that the sample contains at least two points), whereas for $f_{\max}=0$ no missing points are allowed as in spectral calculations.

If $f_{\max}$ is close or equal to 1, a sample containing only a few valid points contributes as much to the variance as a sample of the same size containing many valid points. This applies in particular to large samples (large distances). In the case of scatterometer ocean surface winds this may be the case if the sample is located largely above land. This is not optimal, and can be corrected for by giving the variance of each sample a relative weight w, for instance

$$w=\frac{n-m}{n}, \tag{28}$$

with m the number of missing points in the sample as before.

Finally, structure functions can only be calculated when both end points of the sample (lag) are present. When checking (20) one should thus use only spatial variances from samples that have valid end points.

5. Results and Discussion

Results are shown for all ASCAT-12.5 scatterometer ocean surface vector wind data issued by the Ocean and Sea Ice Satellite Application Facility (OSI SAF) in January 2009. The Advanced Scatterometer (ASCAT) is a C-band radar instrument on board the MetOp-A satellite operated by the European organization for the exploitation of Meteorological Satellites (EUMETSAT). The satellite flies in a polar orbit (inclination 98.702198°) with a period of about 100 min, so most of the Earth is covered in 24 h. More detailed information on ASCAT can be found in *Figa-Saldaña et al.* [2002]. For a more detailed description of the ASCAT-12.5 wind product the reader is referred to *KNMI* [2013]. An overview of daily coverage can be found on www.knmi.nl/scatterometer.

Scatterometer wind products provide horizontal wind speed and direction on a regular grid of Wind Vector Cells (WVCs). The ASCAT grid consists of two swaths each 525 km (42 numbered WVCs) wide and located at either side of the satellite ground track, with a symmetrical gap of about 700 km in-between. No scatterometer winds can be calculated above land, so these points are set to missing. Points were also considered as missing if either the MLE or variational quality control (VarQC) flag was set. The MLE flag indicates the

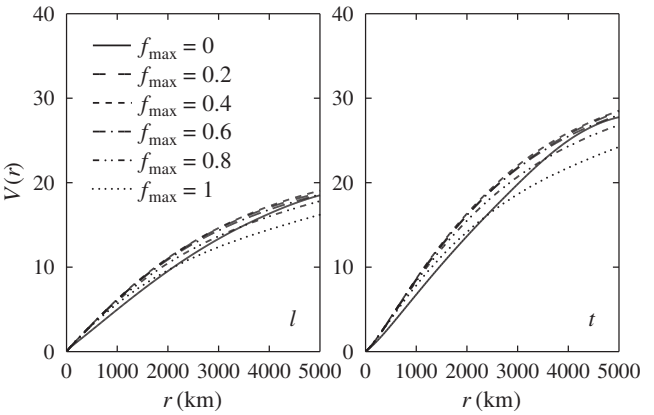

Figure 1. Spatial variances for various values of f_{max} with equal weights for all samples. (left) Results for the along-track wind component *l*, (right) the across-track component *t*.

presence of excessive wind variability, rain splash, or other geophysical anomalies, while the VarQC flag indicates a large spatial inconsistency in the winds.

Scatterometer winds are given in terms of horizontal speed and direction. They were transformed to wind components parallel and perpendicular to the satellite swath, *l* and *t*, respectively, in order to facilitate comparison with structure functions. From the spatial variance perspective such a transformation is not absolutely necessary: transformation to zonal and meridional wind components, *u* and *v*, works equally well.

The results in this section are based on one-dimensional samples of the horizontal wind, with the samples taken in the along-track direction, i.e., for grid cells with the same cross-swath WVC index. One could easily include samples in the cross-track direction, but then the maximum sample size is limited by the scatterometer swath width. The final statistics are averaged over all samples (also over samples with different WVC indices). Ergodicity is assumed here, so that spatiotemporal averages converge to ensemble averages. Note that due to satellite speed, an orbit length of more than 2000 km (approximately 20° of latitude) is covered in 5 min.

5.1. Dependence on Scale and Effects of Sampling Strategy

Figure 1 shows the spatial variances as a function of scale *r* calculated with overlapping samples for various values of f_{max} and with equal weight for all samples. The left-hand plots show the results for the along-track wind component *l*, the right-hand plots for the across-track component *t*. For small to medium scales up to $r \approx 2000$ km, accepting only samples without missing points, $f_{max} = 0$, leads to the lowest estimates for the variance as expected, because this sampling strategy is biased away from meteorologically active areas like fronts and cyclone centers. Nevertheless, the effect is small. Increasing f_{max} leads to an increase in the variance, with the highest variances found for $f_{max} = 0.4$. Further increment decreases the variances, because many samples are accepted that contain a limited number of valid points, for instance samples that are located partially over land. This is supported by Figure 2, which is the same as Figure 1 except that the variance from each sample is weighted with the number of valid points according to (28). Now samples containing many missing points have lower weight, resulting in more uniform behavior of the spatial variance for $f_{max} > 0$. The largest effect of the various sampling strategies in Figures 1 and 2 occurs at scales between 200 and 500 km, and is of the order of 30%. Note that the spatial variances for *t* are higher than those for *l*. This reflects the anisotropy of the global wind field, in particular in the tropical regions which dominate the statistics. Figure 3 shows the effect of requiring that both end points are present in a sample (EPR). The results in Figure 3 were obtained with $f_{max} = 1$, so the number of missing points in a sample is not important. The dotted curves were obtained with dynamic weights (28) and without EPR. They are the same as the dotted curves in Figure 2. The dashed curves were obtained with equal weights. Now the variance at larger scales is reduced by the

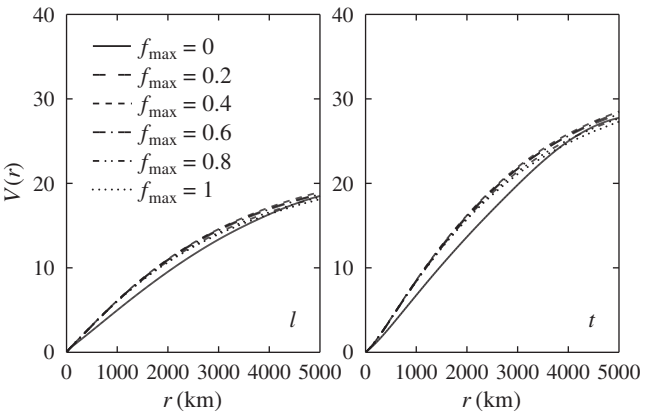

Figure 2. As figure 1, but with dynamic weights.

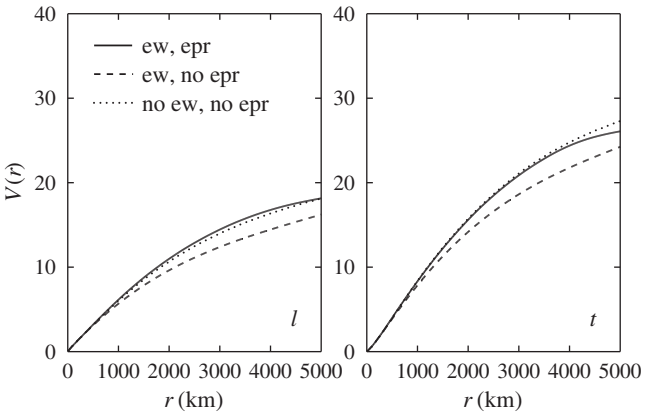

Figure 3. Effect of various sampling strategies, where ew (equal weights) stands for equal weight for each sample and epr (end points required) for rejection of the sample if one or both end points are missing.

influence of samples containing many missing points, in particular samples that lie partly over land. Imposing EPR, solid curves, excludes those samples and the variance increases again.

As indicated by the derivation in Appendix A, one expects relation (20) to hold for nonoverlapping samples without missing points. This is indeed the case (no results shown). For other strategies one expects sampling differences. Figure 4 shows the results for the comparison of spatial variances calculated directly from (18) and (19) (labeled "direct") with those obtained from the second-order structure functions by using (20) (labeled "SF"). The dot-dashed and dotted curves were calculated by accepting all samples ($f_{max}=1$) and imposing equal weight for each sample on the spatial variance calculations. Therefore, spatial variances are calculated for samples with one or both end points missing, whereas these samples do not contribute to the structure functions. As a consequence a considerable difference between the two curves can be observed. The solid and dashed curves were obtained by accepting only samples for spatial variance calculation without missing points ($f_{max}=0$). However, this constraint is not applied to the structure function calculations. The curves are much closer now, but not identical due to sampling differences, with typically 5% differences.

5.2. Tropical Pacific

The form of (14) and (17) suggests to investigate the ratio of the variance over the second-order structure function. The results are shown in Figures 5 and 6, for the wind components *l* and *t*, respectively. The results in Figures 5 and 6 were obtained using overlapping samples with equal weights and a maximum fraction of missing points of 0.1. The figures show results obtained for January 2009 in nine different areas in the Tropical Pacific, for four scatterometer wind products. The areas and scatterometer wind products are the same as studied in [*King et al*., 2015]. The main characteristics of the areas are given in Table 1, and the reader is referred to the aforementioned paper for a more elaborate discussion. It is important to note here that the scatterometer wind products as well as the test areas have different properties, e.g., sensitivity to rain, different structure function slopes, etc.. Nevertheless, Figures 5 and 6 show that the ratio of spatial variance and second-order structure function is more or less constant. All ratios start at a value of 1/4 at lag 1, in agreement with (17). Over each test area the ratios have a value of about 0.2 for both *l* and *t*. For *l* the ASCAT wind products have a slightly higher ratio than the SeaWinds products, whereas for *t* the results for the different wind products are closer together, consistent with the slope results reported in [*King et al*., 2015]. This could be an instrumental effect, because ASCAT and SeaWinds operate at a different radar frequency and have a different observation geometry. Also, SeaWinds is more sensitive to rain than ASCAT, so relatively more cells are rejected by the quality control for SeaWinds than for ASCAT. This may induce sampling effects that play a role.

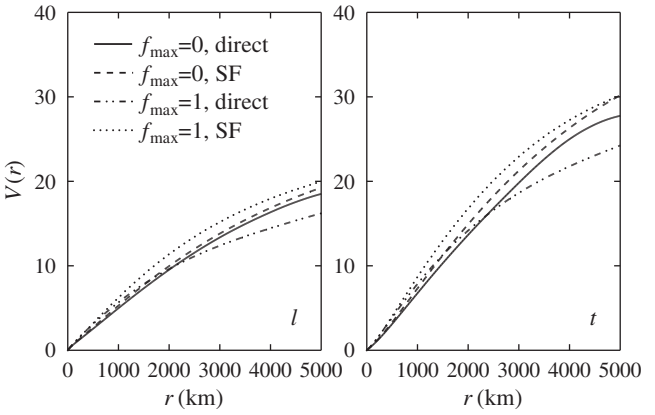

Figure 4. Comparison of directly calculated spatial variances (labeled direct) with those obtained from second-order structure functions (labeled SF).

Figure 7 shows a histogram of all ratio's $V(r)/D(r)$ for *l* and *t* from all nine areas,

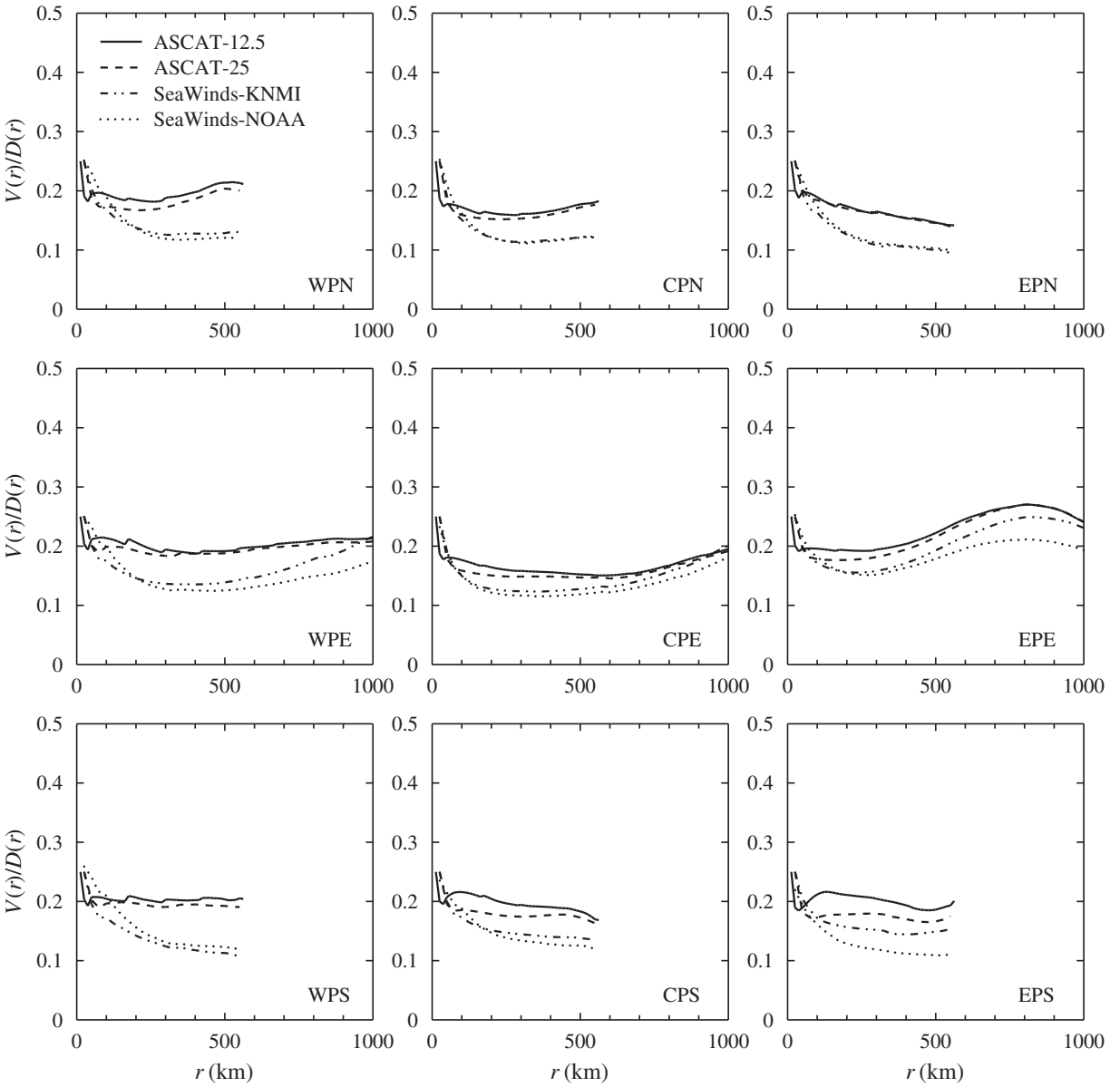

Figure 5. Ratio of spectral variance and second-order structure functions for wind component *l* in January 2009 in nine areas in the Tropical Pacific for four different scatterometer wind products.

all 12 months, all four wind products, and r equal to 100, 200, and 300 km. The average ratio for l is 0.174 with a standard deviation of 0.033, that for t is 0.179 with a standard deviation of 0.031. Assuming a simple power law behavior for the second-order structure function, (26) shows that the power corresponding to these ratio's is 0.95 for l and 0.92 for t. This is a bit higher than the value of 2/3 predicted by classical turbulence theory, but in good agreement with the values found by [*King et al.*, 2015]. Under the same assumptions the wave spectrum behaves as $k^{-1.95}$ for l and $k^{-1.92}$ for t, which agrees well with earlier findings [*Patoux and Brown*, 2001; *Vogelzang et al.*, 2011]. Note that *Patoux and Brown* report higher spectral powers, up to 2.4, but these are found in the extratropics, outside the region of interest in this study.

These results can be summarized, at least for the Tropical Pacific, as

$$V_l(r) \approx 0.17 D_{ll}(r), \quad V_t(r) \approx 0.18 D_{tt}(r). \tag{29}$$

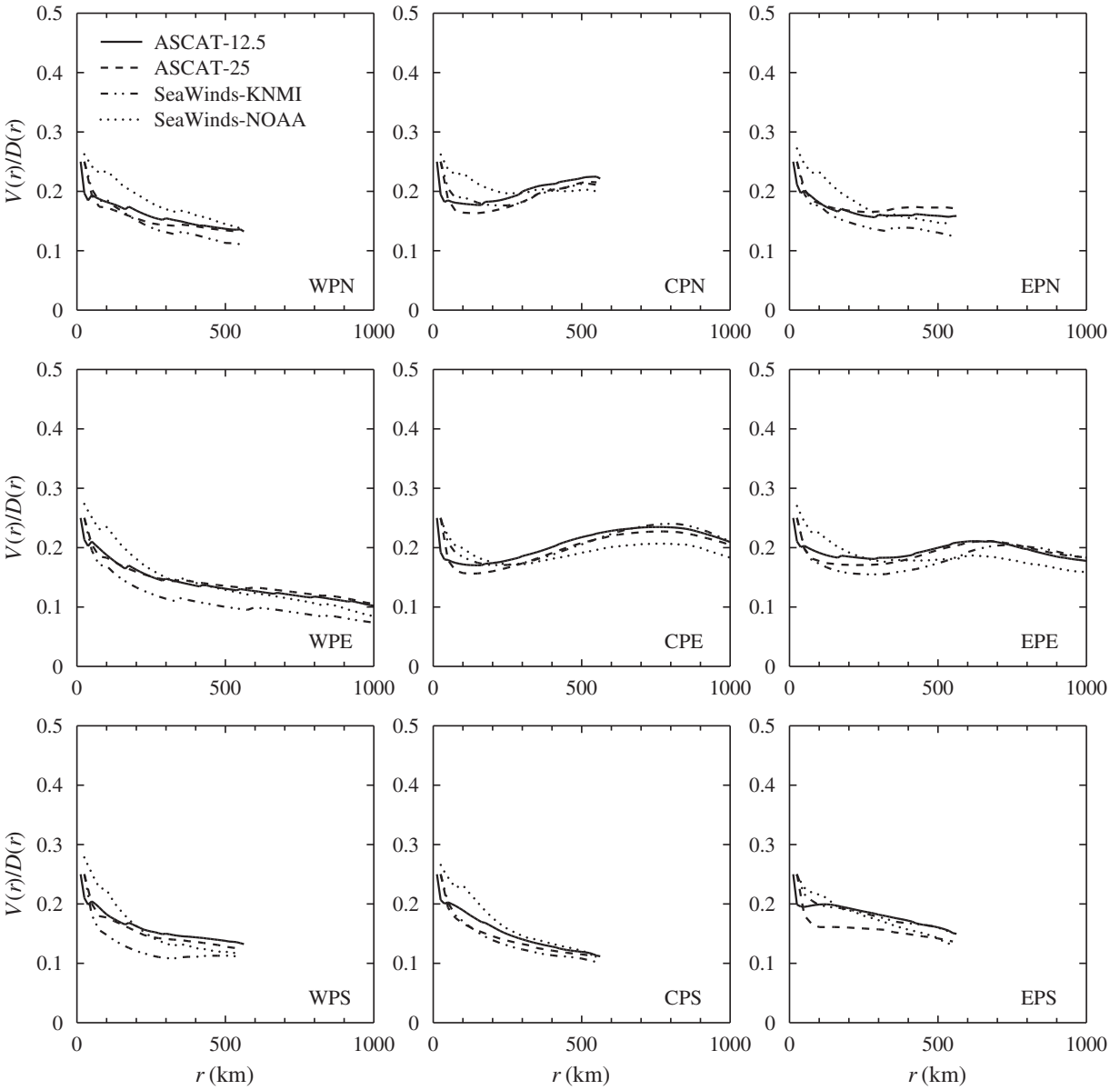

Figure 6. As Figure 5, but for wind component *t*.

5.3. Comparison With Spectral Variance

Interpreting the spectrum as a variance density in the traditional way, variance as a function of scale is given by (7). Figure 8 shows how this relates to spatial variances. The spectra were obtained with the following sampling strategy. Wind values are stored in a buffer of length $n=256$ (spanning about 3000 km for the 12.5 km product) for each Wind Vector Cell (WVC) separately. If a value is missing, the buffer is reset. If the buffer is full, a periodogram is made. The spectrum is the average of all periodograms for all WVC's. The samples are thus nonoverlapping, but with irregular distance between them. Before each periodogram is made the sample is detrended using a linear

Table 1. Geographical Limits and Nomenclature for the Study Regions Shown in Figures 5 and 6

	West Pacific 140°E–180°E	Central Pacific 180°E–220°E	East Pacific 220°E–260°E
North 5°N–10°N	WPN (Rainy)	CPN (Rainy)	EPN (Rainy)
Equatorial 5°S–5°N	WPE (Rainy)	CPE (Dry)	EPE (Dry)
South 10°S–5°S	WPS (Rainy)	CPS (Dry)	EPS (Dry)

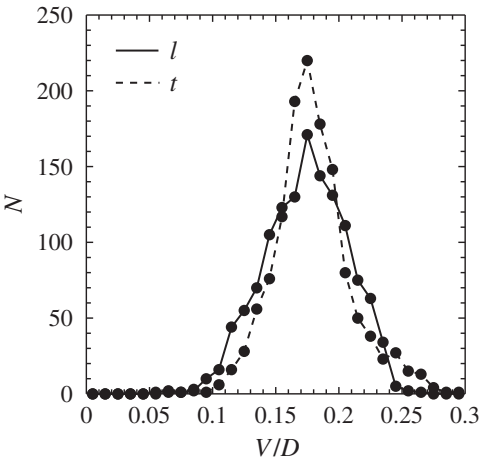

Figure 7. Histograms for the ratio of spectral variance and second-order structure functions for nine areas in the Tropical Pacific, 12 months, and four different scatterometer wind products.

transformation that maps the value of the last point on that of the first point. This detrending transformation has been chosen, because it has relatively small effect on the total variance compared to other detrending methods except first differencing [*Vogelzang et al*., 2011].

The circles in Figure 8 indicate the values of (28) for $r=k_m^{-1}$ with m between 1 and 128. They are connected by the dotted curves to guide the eye. Note that the positions at which the spectral variances are given are strongly concentrated in a small range of scales. The solid curves show the spatial variances calculated using the same sampling strategy, including detrending of each sample, with $f_{\max}=0$ (no missing points allowed) and equal weight for all samples. Though the spectral and spatial variances agree at the largest scale, their behavior at smaller scale is quite different: spatial variances are concave as a function of scale while spectral variances are convex. This is caused by the fact that the Fourier modes that make up the spectrum have no sharp spatial representation.

The dashed curve in Figure 8 is obtained in the same manner as the solid one, but without detrending the samples. Comparison of the solid and dashed curves shows that detrending reduces the variance up to about one third at large scales. At small scales the effect becomes negligible, consistent with the notion that detrending acts as a high-pass filter. The dot-dot-dashed curve is the same as the solid curve in Figure 1 (i.e., overlapping samples with $f_{max}=0$ and equal weights). Note that the dot-dot-dashed curves are close to the dashed ones. This implies that a sampling strategy of nonoverlapping samples without missing points gives about the same results as a sampling strategy of overlapping samples without missing points.

Figure 8 shows that spectral sampling in itself does not produce a strong bias to calm conditions. The restriction to samples without missing points leads to an underestimation of the variance of about 5%, as shown in Figures 1 and 2. A larger effect is introduced by detrending. The detrending method employed here, a linear transformation mapping the first and last point of the sample on the same value, reduces the total sample variance by about one third. This can be overcome by using first differencing. The largest differences between the spectrally calculated spatial variances (dotted curves) and the directly calculated ones are due to invalidity of (7).

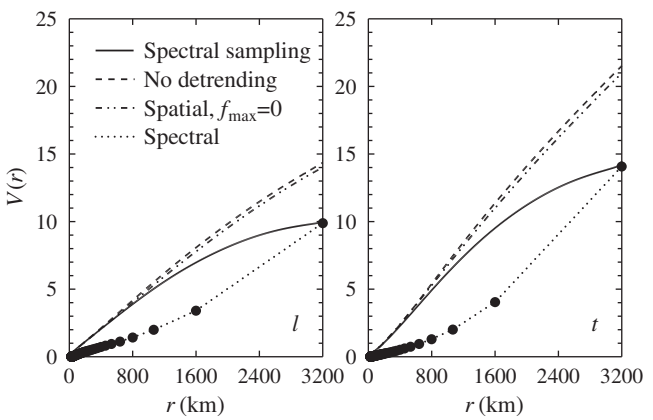

Figure 8. Comparison of spatial variances with spectral variances.

It should be added here that *Vogelzang et al*. [2011] use (7) to calculate representativeness errors as a function of scale for the same four wind products used in this paper: ASCAT-12.5, ASCAT-25, SeaWinds-NOAA, and SeaWinds-KNMI. The spectral integration range is determined by the changes in spectral slope as a function of wave number, and was found to be from infinity to 1/800 km^{-1}. A reanalysis with spatial variance gave the same results (so the conclusions of that study remain valid), but now at a spatial

integration range of 0–200 km. Following *Skamarock* [2004], one would expect that below spatial scales of about 200 km the scatterometer reveals more structure than the model, as observed.

6. Conclusions

Spectral analysis and second-order structure function calculation are common methods to find order-of-magnitude estimates of variance as a function of spatial scale. A quantity called spatial variance offers a more accurate estimate of variance as a function of scale. Spatial variances are also known as M-sample variances. Their interpretation is clear, and they are tolerant of missing data.

It is shown how spatial variances can be related to second-order structure functions, both in the discrete and in the continuous case. For a single data series without missing points this relation, already derived by *Yates* [1948], is statistically exact. As no assumptions are made on the nature of the series, except that it contains finite values, the relation holds also for ensemble averages in cases where velocity differences converge to structure functions. The complement of the spatial variance can be Fourier transformed and related to the spectrum.

The tolerance of spatial variances to missing data points allows investigation of various sampling strategies. In this paper some sampling strategies are tested for ocean surface scatterometer winds from ASCAT on a 12.5 km grid. When using overlapping samples, the relative effect of various choices (maximum fraction of missing points in a sample, requirement that sample end points are not missing, sample weighting) is limited to within 30%. Restricting to samples without missing points, the effect of using nonoverlapping samples (the sampling strategy used for calculating spectra) has little effect compared to using overlapping samples. Therefore spectral sampling of scatterometer winds shows no strong bias to calm conditions.

If the second-order structure function behaves like r^p its ratio with the spatial variance equals $(p+1)(p+2)$. The inverse of this ratio is calculated for nine test areas in the Tropical Pacific and 12 months from November 2008 to October 2009 using four different scatterometer ocean surface wind products. The results show that second-order structure functions are well suited as a proxy for the variance. For the wind field in the Tropical Pacific considered here, the variance equals about 0.17 (0.18) of the structure function value for l (t). This value is consistent with a simple power law behavior of the second-order structure function of the form $r^{-0.95}$ ($r^{-0.92}$), implying a wave spectrum of the form $k^{-1.95}$ ($k^{-1.92}$). These values are in good agreement with earlier results.

Comparison of spatial variances with spectral variances shows good agreement for the variance at a scale equal to the sample length, as expected, but considerable differences at smaller scales. Though the spectrum can be interpreted as a variance density in the spectral domain, it cannot be transformed to a cumulative variance at a sharply defined scale in the spatial domain. Since the spectrum is the Fourier transform of the autocovariance and since autocovariance is related to variance, qualitative arguments based on the integration of the spectrum over a finite interval to yield variances in the spatial domain are correct for well-behaved data sets. Detrending of the samples reduces the variance at large scales, but this can be overcome by using first differencing.

The main recommendation of the paper is thus to use spatial variances if one is interested in an accurate estimation of variance as a function of spatial scale. A first application has been the calculation of representativeness errors in triple collocation exercises. Another application may be analysis of the geophysical errors in scatterometer WVC's as a function of aggregation area size.

Appendix A: Spatial Variance and Second-Order Structure Function

A1. Single Sample

Suppose we have a sample of $l+1$ equidistant points $\{u_i\}=\{u(r_i)\}, i=0,\cdots,l$ taken from a much longer series. The variance of the sample, s_l^2 can be expressed as [see e.g., *Barnes*, 1991]

$$s_l^2=\frac{1}{2(l+1)^2}\sum_{j,k=0}^{l}(u_j-u_k)^2, \tag{A1}$$

where s_l^2 is not considered as an estimator of the variance, but as a measure. When considered as an estimator, (A1) should be multiplied by a factor $(l+1)/l$ in order to arrive at an unbiased estimator. (A1) is symmetric in the summation indices, and the diagonal terms vanish. It can therefore be written as

$$s_l^2 = \frac{1}{(l+1)^2} \sum_{\substack{j,k=0 \\ k>j}}^{l} (u_j - u_k)^2. \tag{A2}$$

A2. Series Averaging

The running average of s_l^2 over the entire series of $n \gg l$ points reads

$$V(l) = \frac{1}{n-l} \sum_{i=1}^{n-l} s_l^2 = \frac{1}{(n-l)(l+1)^2} \sum_{i=1}^{n-l} \sum_{\substack{j,k=0 \\ k>j}}^{l} (u_{i+j} - u_{i+k})^2. \tag{A3}$$

Changing summation variable k to $m=k-j$ and changing the order of the summations, (A3) can be written as

$$V(l) = \frac{1}{(l+1)^2} \sum_{m=1}^{l} \sum_{j=0}^{l-m} \frac{1}{(n-l)} \sum_{i=1}^{n-l} (u_{i+j} - u_{i+j+m})^2. \tag{A4}$$

Now each sum over i can be recognized as the estimator of the second-order structure function, denoted as $D(m)$. For a given value of l the estimation is over subsamples of length $n-l$ with starting points ranging from $i=1$ to $i=l$. The subsamples differ only at their beginning and their end, but the points from $i=l+1$ to $i=n-l-1$ are common. Since $n \gg l$, each sum will converge to the same value $D(m)$ in the limit that $n \to \infty$. Now the summation over j is easily performed, leading to

$$V(l) = \frac{1}{(l+1)^2} \sum_{m=1}^{l} (l+1-m) D(m). \tag{A5}$$

This statistical relationship between spatial variances and structure functions is already given by *Yates* [1948]. It is valid when the data set is free of missing points and large enough to ensure convergence of the ensemble averaging over all samples to a uniform $D(m)$. For $l=1$ the familiar result $V(1) = \frac{1}{4} D(1)$ is obtained.

A direct consequence of (A4) is

$$D(l) = (l+1)^2 V(l) - 2l^2 V(l-1) + (l-1)^2 V(l-2), \tag{A6}$$

with $V(l)=0$ for $l < 1$. This is easily proven by substituting (A5) into the right-hand side of (A6). All terms cancel, except $D(l)$.

A3. Continuous Case

Putting $r_i = i\Delta r \iff i = r_i/\Delta r$, with Δr the grid size, we can introduce the position explicitly in (A5) as

$$V(r_l) = \frac{\Delta r}{r_{l+1}^2} \sum_{m=1}^{l} (r_l - r_{m-1}) D(r_m). \tag{A7}$$

In the limit $\Delta r \to 0$, the summation becomes an integral and the difference between r_{l+1} and r_l vanishes, resulting in

$$V(r) = \frac{1}{r^2} \int_0^r ds (r-s) D(s), \tag{A8}$$

with $r_l \to r$ and $r_m \to s$. Note that $V(r)$ is defined only for $r \geq 0$ by (A8). Since D is an estimator of the second-order structure function, it can be extended to negative values of its argument as an even function, $D(-s)=D(s)$. From (A8) it then follows that also V can be extended as an even function, $V(-r)=V(r)$, as expected.

Relation (A8) can be inverted as follows. Write

$$V(r) = \frac{1}{r} I(r) - \frac{1}{r^2} J(r), \tag{A9}$$

where

$$I(r)=\int_0^r dsD(s), \quad J(r)=\int_0^r dssD(s). \tag{A10}$$

Taking the first and second derivatives of V with respect to r eliminates the integrals $I(r)$ and $J(r)$, and yields the continuous analogue of (A6)

$$D(r)=r^2\frac{d^2V(r)}{dr^2}+4r\frac{dV(r)}{dr}+2V(r). \tag{A11}$$

This can easily be verified by substituting (A9) in (A11). Equation (A11) can also be derived from (A6) by taking the continuous limit in the same way as (A5) led to (A8).

Finally, (A8) has the form of a convolution integral (D. Broomhead, personal communication, 2013), and a change of integral variables from s to $r-s'$ allows it to be written as

$$V(r)=\frac{1}{r^2}\int_0^r ds's'D(r-s'). \tag{A12}$$

A4. Ensemble Averaging

So far, the equations in this appendix were derived for a single, (infinitely) long, discrete or continuous data series. Suppose now that the data were generated by a process for which ensemble averages of spatial differences in u converge to structure functions, in particular

$$D_E(r)=\langle(u(x)-u(x+r))^2\rangle, \tag{A13}$$

with the brackets $\langle.\rangle$ denoting ensemble averaging and the subscript E denoting its result. Consider now the quantity

$$v(x,r)=\frac{1}{r^2}\int_0^r ds(r-s)(u(x)-u(x+s))^2. \tag{A14}$$

Taking an ensemble average yields

$$V_E(r)=\langle v(x,r)\rangle=\frac{1}{r^2}\int_0^r ds(r-s)D_E(s), \tag{A15}$$

because in the right-hand side of (A14) integration and ensemble averaging can be interchanged as both are linear operators, and ensemble averaging only affects the $(u(x)-u(x+s))^2$ term.

Note that (A15) is valid under the assumption that ensemble averages of velocity differences converge to structure functions, an assumption that is valid in this work because the spectrum of ocean surface winds behaves like k^{-p-1} with $1<p<3$. We therefore drop in this paper the distinction between series averaging and ensemble averaging, which is allowed anyway under the assumption of ergodicity. This holds, of course, also for (A5), (A6), (A11), and (A12).

Appendix B: Spatial Variance and Spectrum

From the continuous analogues of (3), (12) and (13) one readily finds

$$\psi(k)=\int_{-\infty}^{\infty} dre^{2\pi ikr}\left[\sigma^2-\frac{1}{2}D(r)\right], \tag{B1}$$

assuming that σ^2 is finite. With $V(r)=\sigma^2-\bar{V}(r)$ equation (23) can be written as

$$D(r)=-r^2\frac{d^2\bar{V}(r)}{dr^2}-4r\frac{d\bar{V}(r)}{dr}+2\left(\sigma^2-\bar{V}(r)\right), \tag{B2}$$

using the fact that $D(r)$, $V(r)$, and $\bar{V}(r)$ can be extended as even functions to negative values of their arguments, see below (A7). Substitution of (B2) into (B1) yields

$$\psi(k)=\int_{-\infty}^{\infty} dre^{2\pi ikr}\left[\frac{1}{2}r^2\frac{d^2\bar{V}(r)}{dr^2}+2r\frac{d\bar{V}(r)}{dr}+\bar{V}(r)\right]. \tag{B3}$$

$\bar{V}$ can be written in terms of its inverse Fourier transform, denoted as $\hat{\bar{V}}$, as

$$\bar{V}(r)=\int_{-\infty}^{\infty} dpe^{-2\pi ipr}\hat{\bar{V}}(p). \tag{B4}$$

From this it easily follows that

$$\frac{d\bar{V}(r)}{dr}=-2\pi i\int_{-\infty}^{\infty} dppe^{-2\pi ipr}\hat{\bar{V}}(p), \tag{B5}$$

$$\frac{d^2\bar{V}(r)}{dr^2}=-4\pi^2\int_{-\infty}^{\infty} dpp^2e^{-2\pi ipr}\hat{\bar{V}}(p). \tag{B6}$$

Substitution of (B4)–(B6) in (B3) and changing the order of the integrations results in

$$\psi(k)=\int_{-\infty}^{\infty} dp\hat{\bar{V}}(p)\int_{-\infty}^{\infty} dr(-2\pi^2r^2p^2-4\pi irp+1)e^{2\pi i(k-p)r}. \tag{B7}$$

Each factor r can be replaced now by a differentiation to k divided by $2\pi i$. Putting the differentiations in front of the integration to r allows this integration to be evaluated. It yields a delta function $\delta(k-p)$ which in turn allows the integration to p to be evaluated. The final result is

$$\psi(k)=\frac{1}{2}k^2\frac{d^2\hat{\bar{V}}(k)}{dk^2}\frac{-2kd\hat{\bar{V}}(k)}{dk}+\hat{\bar{V}}(k). \tag{B8}$$

This shows that the spectrum is not only related to the Fourier transform of the complement of the spatial variance, but also to its first and second derivatives.

Acknowledgments

The ASCAT-12.5 and ASCAT-25 data used in this work can be ordered online from the EUMETSAT Data Centre (http://www.eumetsat.int/website/home/Data/DataDelivery/ EUMETSATDataCentre/index.html) as SAF type data in BUFR or NetCDF format. They can also be ordered from PO.DAAC (http://podaac.jpl.nasa.gov/ datasetlist?ids=Sensor&values=ASCAT&search=) in NetCDF format only. The SeaWinds-NOAA data are also available from PO.DAAC. The SeaWinds-KNMI data are available from the KNMI archive upon an email request to scat@knmi.nl. This work has been funded by EUMETSAT in the context of the Numerical Weather Prediction Satellite Applications Facility (NWP SAF). The contribution of GPK has been supported by EUMETSAT as part of the SAF Visiting Scientists programme. The authors would like to acknowledge the helpful comments of David Broomhead, a treasured friend and inspiration, who died on 24 July 2014 after a long illness.

References

Allan, D. W. (1966), Statistics of atomic frequency standards, *Proc. IEEE, 54*, 221–230. [Available at http://tf.boulder.nist.gov/general/pdf/7.pdf.]

Barnes, R. J. (1991), The variogram sill and the sample variance, *Math. Geol., 23*, 673–678.

Blue, J., and A. Chen (2011), Spatial variance spectrum analysis and its application to unsupervised detection of systematic wafer variations, *IEEE Trans. Autom. Sci. Eng., 8*, 56–66.

Cahalan, R. F., W. Ridgway, W. J. Wiscombe, T. L. Bell, and J. B. Snider (1994), The albedo of fractal stratocumulus clouds. *J. Atmos. Sci., 51*, 2434–2455.

Davidson, P. A., and B. R. Pearson (2005), Identifying turbulent energy distributions in real, rather than Fourier, space, *Phys. Rev. Lett., 95*, 214501.

Figa-Saldaña, J., J. Wilson, E. Attema, R. Gelsthorpe, M. Drinkwater, and A. Stoffelen (2002), The advanced scatterometer (ASCAT) on the meteorological operational (MetOp) platform: A follow on for the European wind scatterometers, *Can. J. Remote Sens., 28*, 404–412, doi:10.5589/m02-035.

Frehlich, R. (2001), Errors for space-based Doppler lidar wind measurements: Definition, performance, and verification, *J. Atmos. Oceanic Technol., 18*, 1749–1772, doi:10.1175/1520-0426(2001)018<1749:EFSBDL>2.0.CO;2.

Frehlich, R., L. Cornman, and R. Sharman (2001), Simulation of three-dimensional turbulent velocity fields, *J. Appl. Meteorol., 40*, 246–258.

Freilich, M. H., and D. B. Chelton (1986), Wavenumber spectra of Pacific winds measured by the Seasat scatterometer, *J. Phys. Oceanogr., 16*, 751–757.

Frisch, U. (1995), *Turbulence*, Cambridge Univ. Press, Cambridge, Mass.

Kahn, B. H., and J. Teixeira (2009), A global climatology of temperature and water vapour, *J. Clim., 22*, 5558–5575.

King, G. P., J. Vogelzang, and A. Stoffelen (2015), Second-order structure function analysis of scatterometer winds over the Tropical Pacific, *J. Geophys. Res. Oceans, 120*, doi:10.1002/2014JC009992.

KNMI (2013), *ASCAT Wind Product User Manual*, EUMETSAT OSI SAF report SAF/OSI/CDOP/KNMI/TEC/MA/126, KNMI, De Bilt, Netherlands. [Available at www.knmi.nl/scatterometer.]

Lorenc, A. C. (1986), Analysis methods for numerical weather prediction, *Q. J. R. Meteorol. Soc., 112*, 1177–1194.

Lorenz, E. N. (1979), Forced and free variations of weather and climate, *J. Atmos. Sci., 36*, 1367–1376.

Mahadevan, A., and J. W. Campbell (2002), Biochemical patchiness at the sea surface, *Geophys. Res. Lett., 29*(19), 1926, doi:10.1029/2001GL014116.

Nastrom, G. D., and K. S. Gage (1985), A climatology of atmospheric wavenumber spectra of wind and temperature observed by commercial aircraft, *J. Atmos. Sci.*, *42*, 950–960.

Patoux, J., and R. A. Brown (2001), Spectral analysis of QuikSCAT surface winds and two-dimensional turbulence, *J. Geophys. Res.*, *106* (D20), 23,995–24,005, doi:10.1029/2000JD000027.

Percival, D. B., and A. T. Walden (1993), *Spectral Analysis for Physical Applications*, Cambridge Univ. Press, Cambridge, U. K.

Press, W. H., B. P. Flannery, S. A. Teukolsky, and W. T. Vetterling (1988), *Numerical Recipes in C*, Cambridge Univ. Press, Cambridge, U. K.

Skamarock, W. C. (2004), Evaluating mesoscale NWP models using kinetic energy spectra, *Mon. Weather Rev.*, *132*, 3019–3032, doi:10.1175/MWR2830.1.

Stoffelen, A., and D. Anderson (1997), Scatterometer data interpretation: Estimation and validation of the transfer function CMOD4, *J. Geophys. Res.*, *102*(C3), 5767–5780, doi:10.1029/96JC02860.

Vogelzang, J., A. Stoffelen, A. Verhoef, and J. Figa-Saldaña (2011), On the quality of high-resolution scatterometer winds, *J. Geophys. Res.*, *116*, C10033, doi:10.1029/2010JC006640.

Yates, F. (1948), Systematic sampling, *Philos. Trans. R. Soc. London A*, *241*, 345–377, doi:10.1098/rsta.1948.0023.